ORNL/TM-2018/1029

Tensile and Microstructure Characterization of SNS Target Swirl Bubblers Fabricated by Additive Manufacturing

David McClintock
Thao Strong
Drew Winder

October 2018

OAK RIDGE NATIONAL LABORATORY
MANAGED BY UT-BATTELLE FOR THE US DEPARTMENT OF ENERGY

ORNL/TM-2018/1029

Neutron Technologies Division
Spallation Neutron Source
Oak Ridge National Laboratory

TENSILE AND MICROSTRUCTURAL CHARACTERIZATION OF SNS TARGET SWIRL BUBBLERS FABRICATED BY ADDITIVE MANUFACTURING

David McClintock
Thao Strong
Drew Winder

Date Published: October 2018

Prepared by
OAK RIDGE NATIONAL LABORATORY
Oak Ridge, TN 37831-6283
managed by
UT-BATTELLE, LLC
for the
US DEPARTMENT OF ENERGY
under contract DE-AC05-00OR22725

CONTENTS

ABSTRACT

During operation the mercury facing surfaces of the Spallation Neutron Source target vessel are damaged by cavitation-induced erosion. One option to decrease the erosion damage is to decrease the intensity of the proton-induced pressure waves using small gas bubble mitigation. Injection of small diameter helium bubbles into mercury has been shown in decrease the intensity of proton-induced pressure waves and mitigate erosion damage to mercury/vessel interface surfaces. Several bubbler designs have been evaluated for implementation in the SNS target. One promising bubbler design is called a swirl bubbler, which is capable of producing a high density of small diameter helium bubbles in flowing mercury. Due to the complexity of the swirl bubbler design and the geometric restrictions of conventional machining processes, additive manufacturing was considered for fabrication. However, there were uncertainties with the mechanical properties of bubblers fabricated with additive manufacturing. A series of experiments were designed to characterize the tensile properties and microstructure of swirl bubblers fabricated using selective laser melting (SLM), both before and after consolidation via hot isostatic pressing (HIPing). This report summarizes the tensile and microstructural characterization of HIPed and non-HIPed swirl bubblers produced via the SLM process. The results show that the as-fabricated material contained appreciable porosity, lack-of-fusion defects, and inconsistent tensile properties with essentially zero ductility. After a HIPing treatment the microstructure became fully consolidated, and the tensile properties surpassed the requirements specified in the material standard for steel-mill produced 316L plate material used to fabricate the SNS target vessel. While further testing is recommended to evaluate the material's susceptibility to fatigue fracture, these results indicate 316L bubbler assemblies produced using SLM and HIPed are promising candidates for implementation in a future SNS target module.

1. INTRODUCTION

Flowing mercury is the neutron-producing target material at the Spallation Neutron Source (SNS). The mercury flows through a 316L stainless steel target module where the proton beam interacts with the mercury to produce neutrons via spallation reactions for use in the facility's instruments. Mercury is an excellent spallation neutron target material due to its large atomic number and physical characteristics, specifically that it is a liquid metal with high thermal conductivity and heat removal capacity. But mercury has a significant issue when implemented in a short-pulse spallation neutron system due to the interactions between the proton beam, mercury, and target structure.

When a proton pulse enters the SNS target module the energy is almost instantaneously deposited, causing rapid (10^{-7} K/s) isochoric heating of the mercury. The sudden heating produces compression waves in the mercury that propagate out from the proton-beam interaction zone toward the vessel structure. Upon reaching the vessel surfaces, the compression waves are rarefied and transformed into tensile pressure waves that propagate back through the mercury. If the tensile pressure waves are intense enough, the mercury will cavitate into a gaseous phase, where mercury vapor bubbles nucleate, grow to a maximum size, and collapse. During the collapse event of a near-wall bubble, constraint of the mercury around the bubble may form a high-velocity mercury jet that can pierce and propagate through the bubble, as shown in Figure 1. If the collapse occurs at or near the vessel surface the high-velocity jet can erode material from the vessel through either direct removal of material or fatigue fracture from repeated impacts of shockwaves from the bubble collapse events. The process of material removal from the interior surface of the mercury target vessel is called *cavitation-induced erosion* [1].

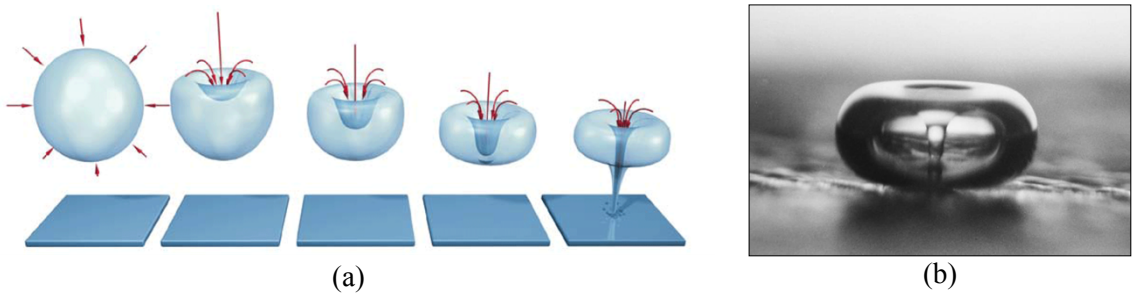

(a) (b)

Figure 1. (a) Schematic of the cavitation-bubble growth and collapse lifecycle [Figure Credit: http.eswt.net/cavitation] and (b) photograph of a high-velocity jet piercing a cavitation bubble and impinging on a container surface in water [Photo Credit: Lawrence Crum (University of Washington)].

Researchers at the Japan Atomic Research Institute (JAERI), renamed Japan Atomic Energy Agency (JAEA) in 2005, were among the first to identify cavitation-induced erosion as a possible life-limiting process for short-pulsed liquid metal spallation targets [2]. Following the recognition that cavitation-induced erosion might be an issue for short-pulse liquid metal spallation targets, a significant amount of research was conducted to better understand the factors influencing cavitation-induced erosion and techniques to mitigate or delay the erosion damage [1-7]. Experiments conducted at the Los Alamos Neutron Science Center's (LANSCE) Weapons Neutron Research (WNR) facility in 2001 verified that cavitation-induced erosion to a container vessel surface could be produced by proton beam injection into

mercury [3]. Tests at WNR were also used to evaluate the influence of container geometry and surface hardening treatments on erosion damage caused by proton beam injection into mercury [4].

Following the in-beam testing several experiments with a vibratory horn test apparatus were conducted to evaluate surface hardening treatments for the SNS target vessel [5,7]. These experiments showed that surface hardening treatments increased the incubation period for erosion damage, where little or no significant erosion occurs. A surface-hardening treatment called Kolsterising® was shown to be the most effective treatment to increase the incubation phase, and was selected to treat the mercury-facing surfaces of SNS target vessels. While surface hardening can increase the target lifetime by delaying the onset of steady-state erosion, it does not prevent or completely mitigate erosion damage. In order to prevent erosion damage other techniques are necessary that interrupt the cavitation bubble growth/collapse process or reduce the energy available to the cavitation bubble growth/collapse process.

The most promising cavitation-induced erosion mitigation techniques evaluated during research and development for the SNS target module were: mitigation through fluid flow against the vessel surfaces [8,9], mitigation using a gas wall or bubbly curtain against the vessel surfaces [10,11] and mitigation by small bubble gas injection into the bulk mercury flow [1,10,12]. Several series of experiments were performed at the WNR facility to evaluate the effectiveness of the various mitigation techniques using proton pulses with energy densities and induced-pressure conditions prototypic to the SNS mercury vessel.

Early experiments performed in 2005 at WNR demonstrated the effect of flow on cavitation-induced erosion damage, where results showed flow reduced the observed damage by half compared to specimens tested in stagnant mercury [8]. Later experiments confirmed that flow was "somewhat effective" at reducing erosion damage [12], but the erosion mitigation of flow appeared to be less effective compared to gas wall and gas bubble injection techniques. The mitigating effect of flow was utilized in a variant of the original SNS target module called the *Jet-flow* target design. The jet-flow target was designed to create a high-velocity (2-3 m/s) flow of mercury against the inner window section where the proton beam enters the target, as shown in Figure 2.

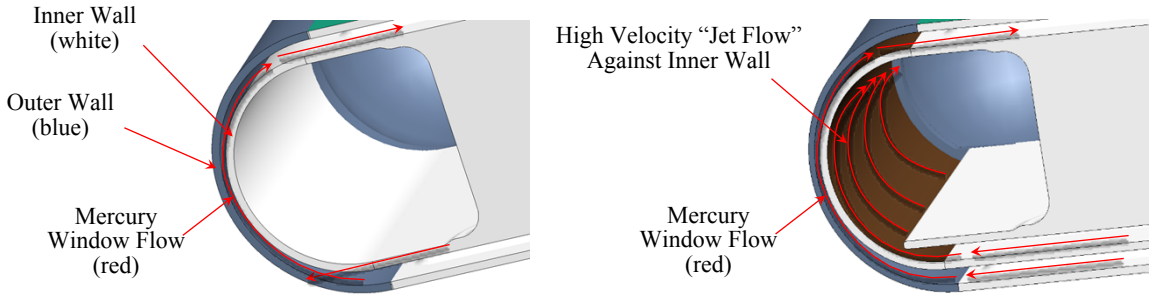

Figure 2. Cross-sectional side view of the beam entrance region (a) original and (b) the jet-flow target designs.

The first jet-flow target operated was Target 10, which developed a leak during operation at a weld joining the front body and transition sections after only 601 MW-hr. Coincidentally, Target 6, an original design target, also developed a leak at almost the same total absorbed energy as Target 10. These two targets provided a direct comparison of erosion damage between original and jet-flow target designs that

experienced almost identical operational conditions. Photographs of samples from the inner window of Target 6 and 10 showed the damage to Target 6 was more severe compared to the Target 10 inner wall, as shown in Figure 3. Also, the erosion damage to the center of the Target 10 inner wall was different from previous erosion damage patterns, with two small patches present on the Target 10 sample and no I-shaped erosion pattern typically observed on samples of original design targets.

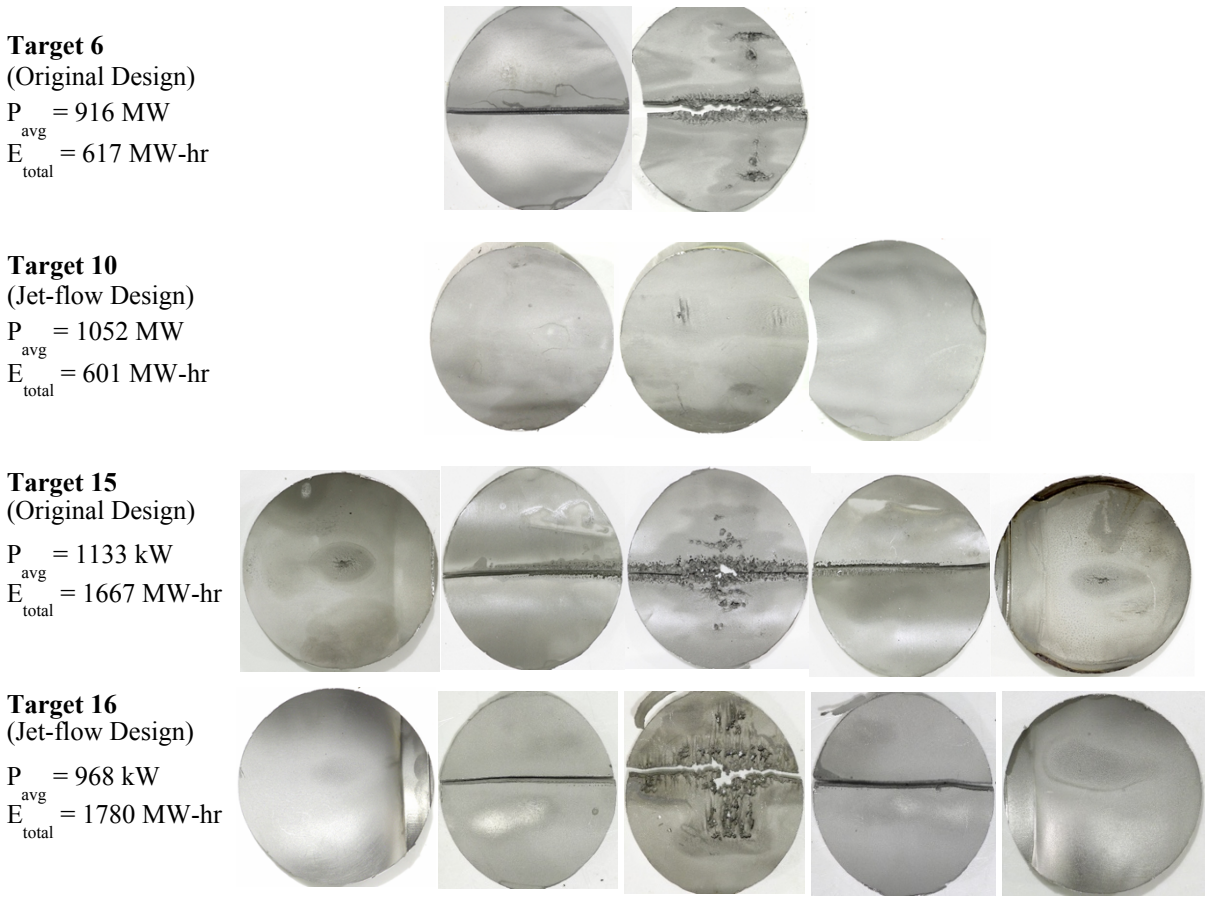

Figure 3. Photographs comparing the erosion damage to the mercury vessel inner wall in both an original (Targets 6 and 15) and jet-flow (Target 10 and 16) target designs after service.

The second jet-flow target operated was Target 16, which was operated to 1780 MW-hr at an average power of approximately 968 kW. The severity of erosion damage to the inner wall of Target 16 was similar to original design targets (Target 15) that had similar operational histories, as shown in Figure 4, although the morphology of the erosion pattern in Target 16 was different from original design targets. The damage to the Target 16 inner wall was oriented parallel to the direction of the jet flow and was more pronounced on the "down-stream" section of the inner wall (top of sample in Figure 4). Observations of damage to the Target 16 jet-flow inner wall were discouraging and indicated that erosion mitigation using fluid flow was not effective at protecting the inner wall of targets operated at appreciable total energies ($\gtrsim$1500 MW-hr).

During early research on cavitation-induced erosion mitigation techniques, experts in the field of acoustics recommended research into a technique commonly used in naval vessels to reduce and obscure the sound emitted by ships during operation as a possible mitigation technology for the SNS target, namely

creation of a gas-wall or gas-curtain. To hide the acoustic emissions from enemy ships, a gas-injection system called a *masker* is used to surround the noisiest parts of the ship with a wall of small gas bubbles, which impede the transmission of sound waves from the ship to the water. This technique might be feasible to protect the inner wall of the mercury target vessel from cavitation-induced erosion. But a gas wall would likely interfere with a jet-flow against the inner wall, which when used together might reduce the mitigating effect of both techniques. Also, implementation of a gas wall in an actual target vessel is complicated due to the design and fabrication requirements of the SNS target. Therefore, more research is necessary to determine the efficacy of gas-wall protection and the possible competition between mitigation mechanisms before its implementation.

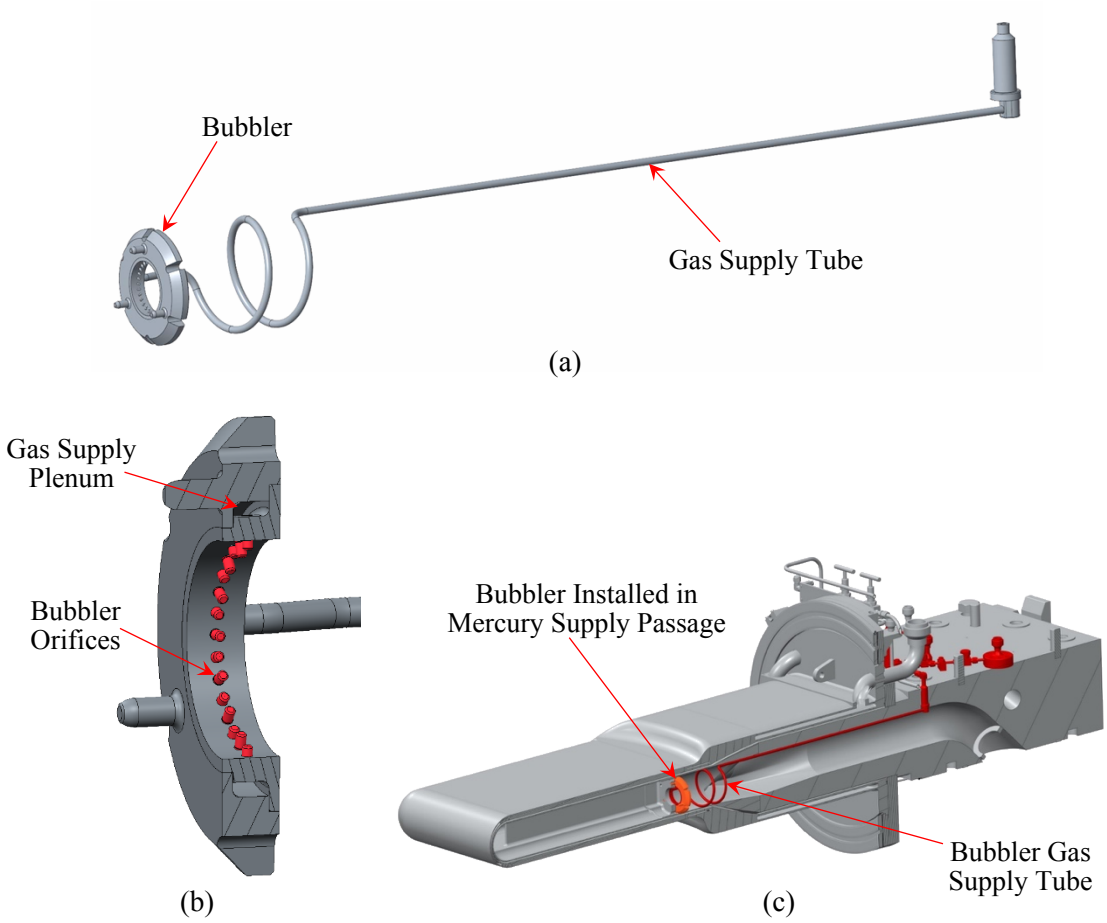

Figure 4. (a) Illustration of SNS orifice bubbler assembly (b) cross-sectional view of an SNS target orifice bubbler and (c) sectioned view of a bubbler assembly installed in a target supply passage.

The cavitation-induced erosion mitigation technique that appears most promising is injection of small bubbles in the bulk mercury flow. Small bubble injection is attractive for several reasons: the geometry and fabrication methods used for SNS targets allows bubblers to be easily incorporated into the design, injection of small bubbles reduces the strain/stress imposed on the target vessel structure [8], and injection of small bubbles has been shown to greatly reduce erosion damage [1,8,10,12,13]. Tests performed in 2002 and 2005 at WNR tested the effect of small bubble gas injection on erosion damage, and it was shown that

injecting a small amount of helium gas bubbles reduced the damage by a factor of four compared to specimens tested in stagnant mercury [1,8].

The large decrease in erosion damage observed during gas bubble injection experiments led to further development of a bubble generator (bubbler) suitable for incorporation into the SNS target design. There are several types of bubblers capable of injecting gas into the mercury flowing through the target vessel. The requirements for an appropriate bubbler include: the ability generate a high number density (gas volume fraction 10^{-5} – 10^{-4}) of small bubbles (diameter <150 μm), the pressure drop from the bubbler(s) in the mercury flow passage must be low enough to permit balancing with other target design changes, and the bubbler(s) design, including geometry and gas supply requirements, must be feasible for incorporation into the SNS target design. Although a variety of bubbler types were investigated, only two bubbler designs were chosen for development and possible implementation in an SNS target [12]: an orifice bubbler developed by the SNS R&D team and a swirl bubbler design developed by collaborators at the Japan Proton Accelerator Research Complex (J-PARC) [14].

The orifice bubbler design produces bubbles by flowing gas through a series of small holes (diameter ~8 μm) fabricated into small cylinders arranged in a circular pattern on a ring-shaped structure. Helium is supplied through a fitting in the target manifold block to a long tube that transports the gas to the bubbler. The supply tube has a spiral shape toward the end that attaches to the bubbler to relax tolerances on the tube length and accommodate movement of the tube during operation. A plenum structure inside the bubbler provides gas to the orifices. The gas flow through the bubbler orifices is "choked" and the flow rate is pressure-controlled during operation.

The first SNS targets operated with small bubble gas injection were equipped with orifice bubblers. Due to the simplicity of the orifice bubbler, minimal modifications were required to the target design and targets already in the fabrication process could be retrofitted with orifice bubbler assemblies. Targets 16 and 17 were both equipped with orifice bubblers, but gas was not injected during operation of these two targets; they were intended to test the robustness of the bubbler assemblies during operation. Target 18 was the first target to operate with gas injection using orifice bubblers, and was operated with a modest gas injection rate of approximately 0.3 standard liters per minute (SLPM). The mercury vessel inner windows of Target 16, a jet-flow target design operated without gas injection, and Target 18 are shown in Figure 5. The erosion damage to the inner wall was reduced in Target 18, as were vessel strain values measured by strain sensors attached to the mercury vessel during operation [15]. These results were encouraging and prompted an effort to expedite implementation of higher gas injection rates on future targets.

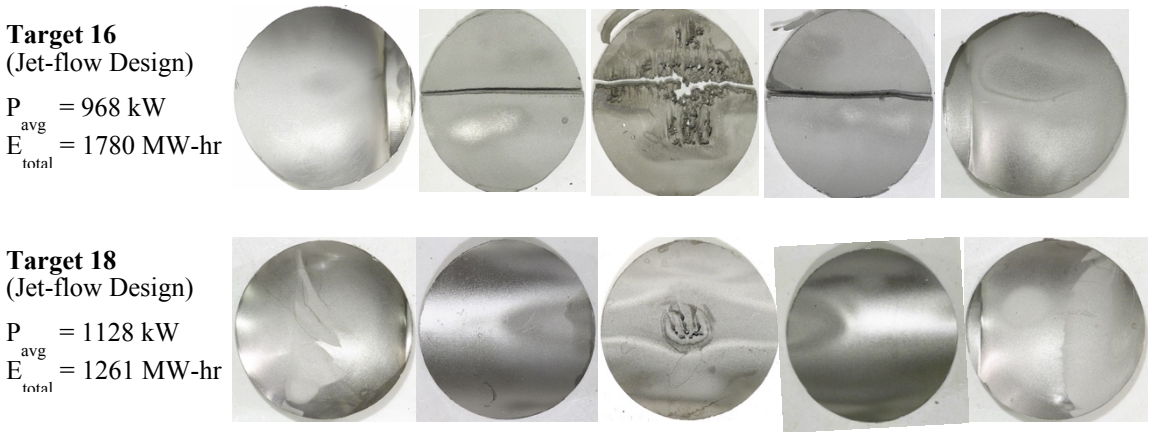

Figure 5. Photographs of specimens removed from the mercury vessel inner walls of Target 16 (jet-flow without gas injection) and Target 18 (jet-flow with gas injection) after operation.

The swirl bubbler design developed by researchers at J-PARC, shown in Figure 6, is a more appropriate bubbler for higher gas flow rates (>2 SLPM), and is effective at producing a high number of small bubbles (diameter ~20-150 μm) distributed throughout the downstream flow. Swirl bubblers produce bubbles by injecting gas into the center of a vortex created by stationary swirl vanes and exploiting the Coanda effect, which shears the bubbles to produce micro size bubbles. Swirl bubblers can also be operated in flow-rate control mode, whereas orifice bubblers are operated with a "choked flow" that is controlled via pressure. Operating the bubblers via flow-rate allows more precise control over the gas injection rate. Additionally, the swirl bubbler design is less likely to clog compared to the orifice bubbler design, due to the larger gas supply passages in swirl bubblers and the downstream facing gas supply port. While swirl bubblers have several advantages they cannot be retrofit into a "standard" SNS target design after fabrication; swirl bubblers must be included in targets during fabrication.

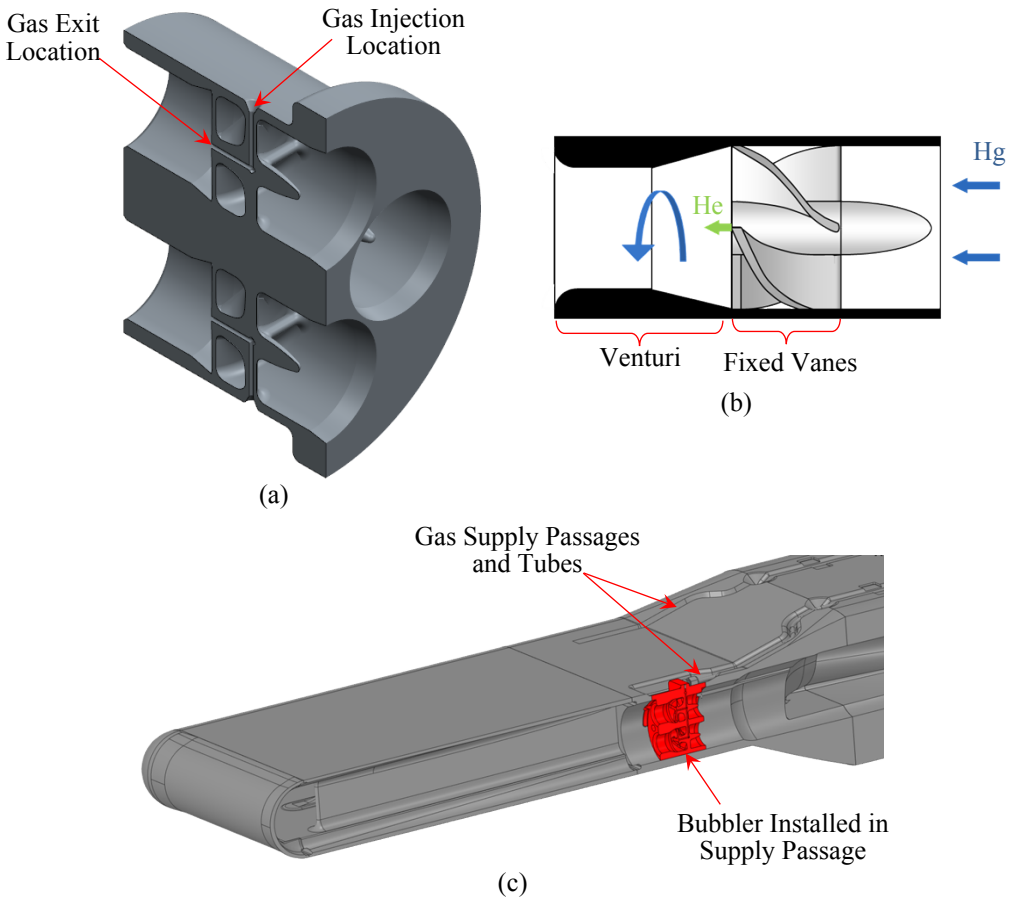

Figure 6. (a) Cross-sectional view of a swirl bubbler assembly, (b) diagram showing the flow pathway through the bubbler, and (c) cross-sectional view of bubbler assembly installed in a target.

Efforts are currently underway to finalize the design of an SNS target that incorporates swirl bubblers called the *Chinstrap* target design. Part of the design evaluation for the Chinstrap target is the fabrication methods available to produce the swirl bubblers. There are two basic fabrication pathways for the swirl bubbler design: conventional machining and welding of stainless steel plate material, or additive manufacturing via laser sintering of stainless steel. Conventional machining, where material is removed from a section of material using cutting tools and electrical discharge machining, can be used to fabricate the bubblers but requires high-precision machining and welding capabilities. Whereas, additive manufacturing can be used to fabricate the near final bubbler shape without welding or complicated multi-step machining processes. Although components can be quickly fabricated using additive manufacturing, the as-deposited microstructure is highly porous and must be treated with a consolidation process called hot isostatic pressing (HIPing) to increase the strength, ductility, fatigue strength, and fracture toughness of the component.

Due to the potential advantages of fabricating swirl bubblers using additive manufacturing, staff in the Source Development Group at the SNS are researching the feasibility of using additive manufacturing to produce the SNS target swirl bubblers. This report presents the microstructural and tensile characterization

of swirl bubblers that were fabricated from 316L using additive manufacturing, both before and after consolidation via HIPing.

2. EXPERIMENTAL PROCEDURE

2.1 BUBBLER FABRICATION

Two swirl bubbler assemblies were produced using additive manufacturing at the Oak Ridge National Laboratory Manufacturing Demonstration Facility (MDF) in Knoxville, Tennessee. The bubblers were fabricated from 316L powder that was consolidated by selective laser melting (SLM) using a Renishaw AM250 with PlusPac™ operated using the parameters shown in Table 1. The powder used for the bubblers was a mixture of powders from different suppliers, but was primarily composed of a Renishaw 316L powder (part number 790101001). The powder mixture was sieved to produce a diameter size distribution of 15-45 μm.

Parameter	Value
Beam Power	200 W
Point Spacing	60 μm
Exposure Time	80 microseconds
Effective Velocity	0.64 m/s
Hatch Spacing	110 μm
Focus Offset	0.0 mm

Table 1. Laser melting parameters used to fabricate the SNS swirl bubblers.

The swirl bubblers were fabricated on a thick steel "build plate" composed of low-carbon steel, as shown in Figure 7. During the build process metal powder is spread over the surface of the build plate and the component is produced by melting selective areas of the powder layer. After a layer is consolidated with the laser scan, another layer of powder is spread over the build plate and another layer is consolidated via scanned laser. This process is continued until the entire part is built, which produces a "layered" surface finish as shown in Figure 7 (b).

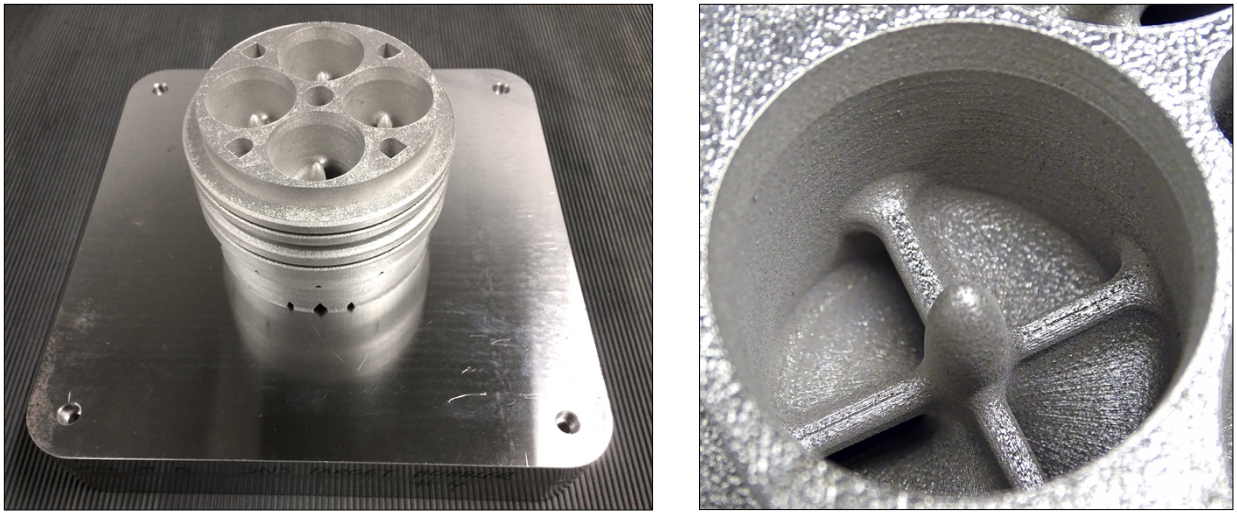

(a) (b)

Figure 7. (a) SNS swirl bubbler as-fabricated on the build plate and (b) a closeup image of one of the swirl bubbler passages.

One of the issues with components produced using additive manufacturing consolidated via laser melting is microstructure porosity. As powder particles are melted together, voids or pores form between the melting powder spheres and the previously deposited layer when the particles are not fully melted by the laser. The porosity in the microstructure acts as crack initiation sites and decrease the fracture toughness and fatigue resistance of material produced from SLM. Therefore, metal parts produced using additive manufacturing processes that require high strength and resistance to fatigue and fracture failure are consolidated using hot isostatic pressing (HIPing). HIPing is a material-consolidation treatment where components are placed in a pressure chamber and exposed to high temperature and pressures for a prescribed period of time. The pressure from the inert gas, usually argon, at elevated temperatures causes the component to be compressed uniformly from all directions and deform plastically. The plastic deformation causes voids and cavities in the microstructure to collapse, which consolidates the material to near theoretical density and improves the mechanical properties to values similar to conventional wrought material forms.

One of the SNS swirl bubblers produced by SLM was treated using the HIPing process by Bodycote (Princeton, KY, USA). The swirl bubbler was HIPed at a temperature of 1135°C and a chamber pressure of 103.4 ±1.7 MPa for 4 hours. During the HIPing process chemical reactions on the surface of the bubbler with impurities in the HIPing chamber caused the bubbler to become green in color, as shown in Figure 8. Prior to specimen fabrication, the bubblers were removed from the build plates using a band saw and the height dimension was established by a final machining operation on the cut surface that was formerly bonded to the build plate.

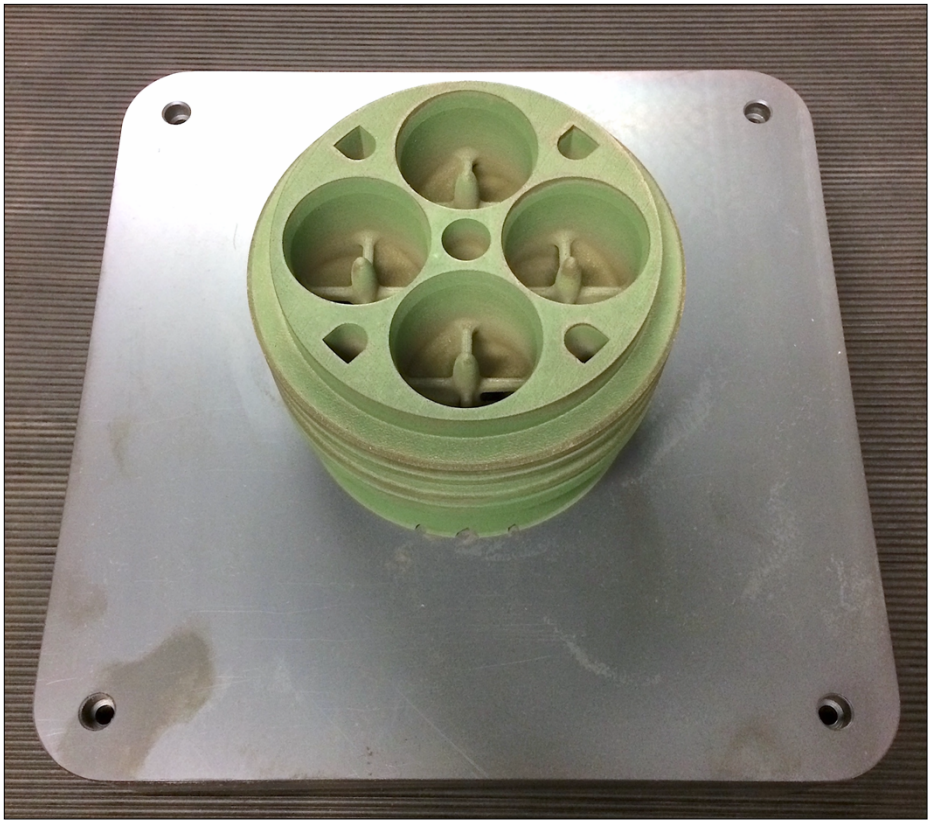

Figure 8. Discolored SNS swirl bubbler and build plate after HIPing treatment.

2.2 SPECIMEN FABRICATION

Two specimen types were fabricated and tested during this characterization campaign: "SS-3" type tensile specimens and rectangular microstructure characterization specimens. The drawings for the SS-3 and microstructure characterization specimen designs are shown in Figure 9. Specimens were machined from several different areas of the swirl bubblers to quantify any variations in mechanical properties or microstructure associated with different regions of the bubblers. Detailed machining maps were produced for each bubbler assembly, which are included in Appendix A.

2.3 SPECIMEN TESTING AND CHARACTERIZATION

Tensile specimens were tested at room temperature using a shoulder-loading specimen holder, shown in Figure 10. Specimens were tested using a constant strain rate of 10^{-3} s^{-1}. Microstructural characterization blanks were mounted in clear-epoxy metallurgical mount, ground, and polished following the procedure shown in Table 2. Specimens were lightly etched immediately after polishing using Glyceregia (20 ml glycerol + 30 ml hydrochloric acid + 10 ml nitric acid) for approximately 1 minute via manual swabbing with a cotton ball.

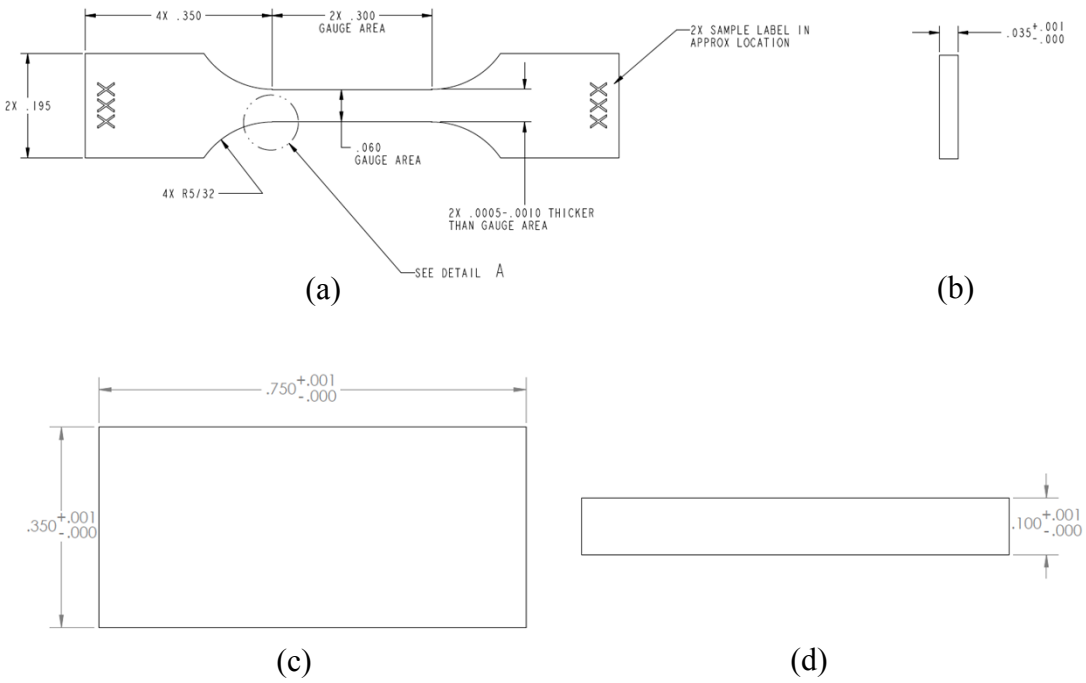

Figure 9. (a) Top and (b) side view of SS-3 tensile specimen design, and (c) top and (d) side view of microstructure characterization specimen design. All dimensions are shown in inches.

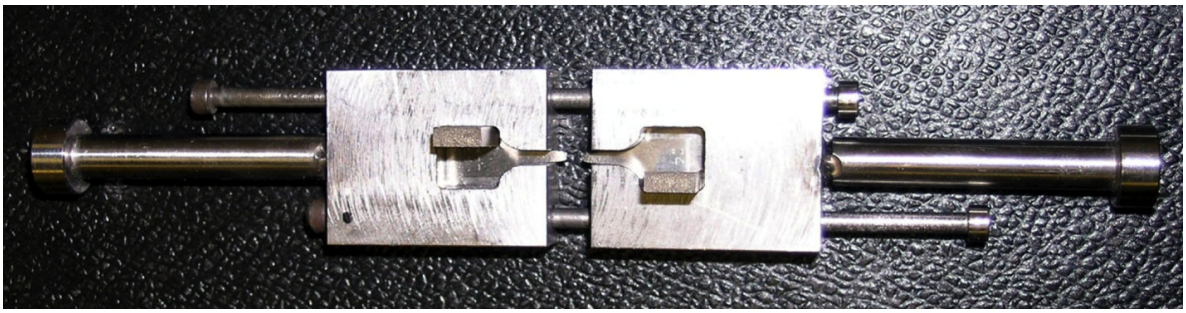

Figure 10. Picture of shoulder-loading specimen holder designed to test SS-3 tensile specimens.

Step 1	Mount specimen in clear epoxy
Step 2	Grind to 4000 Grit
Step 3	Polish with Allegro disc with 6 µm diamond
Step 4	Polish with Largo disc with 6 µm diamond
Step 5	Polish with DAC cloth disc with 3 µm diamond
Step 6	Polish with NAP cloth disc with 1 µm diamond

Table 2. Metallurgical specimen preparation procedure.

After a final polish, optical images of the microstructure were obtained at various magnification levels for each microstructure characterization specimen. The images were analyzed using the software analysis program ImageJ to calculate the percent porosity for each specimen. The areas of porosity in each image were selected using the "Threshold" function (under the "Image → Adjust" tab) to select the darkest 4-6% of the black/white scale. The percentage of porosity for each specimen was calculated using the "Analyze Particles…" function from the "Analyze" tab, which calculates a percent area for microstructural features highlighted using the "Threshold" function. Circularity settings of 0-1.0 and 0.50-1.0 were used for the as-fabricated and HIPed bubblers, respectively, to reduce the contribution from the grain boundary contrast.

3. RESULTS AND DISCUSSION

3.1 MICROSTRUCTURE CHARACTERIZATION

Representative images of the microstructure for the as-fabricated swirl bubbler are shown in Figure 11 at increasing magnification levels. The layered nature of the microstructure is clearly visible in the optical-micrograph images, and the porosity inherent to this fabrication technique are discernable as irregularly shaped black regions in the micrographs. A fan-shaped morphology was observed throughout the microstructure, which is due to the hemispherical geometry of the melt pool created by the energy deposition from the laser, and the overlapping nature of each successively deposited layers. Also, visible in Figure 11 (d) is the micron-scale cellular-dendritic morphology created in the microstructure by the rapid melting and solidification of the SLM process.

Several regions with incomplete melting were observed in the micrographs of the as-fabricated swirl bubbler assembly, as shown in Figure 12. These regions where large cavities form are generally referred to as lack-of-fusion defects, and occur when the powder is partially melted due to insufficient energy density in the laser-powder interaction region. Insufficient energy density during fabrication is likely due to the settings used during the build process, which were not optimized for the swirl bubbler production.

The melt energy density used for both swirl bubblers was based on optimal settings for a small cube of material, usually 1 cm^3, built directly on a substrate (build plate). The melt energy density settings optimized for building directly on the substrate was used throughout the entire build, and no adjustments were made for the different geometry and thicknesses encountered at different locations in the bubbler assemblies. Since the bubblers are tall and the geometry varies greatly throughout the part, using the same melt energy density setting for an entire bubbler is not ideal, and can produce lack-of-fusion defects in the microstructure.

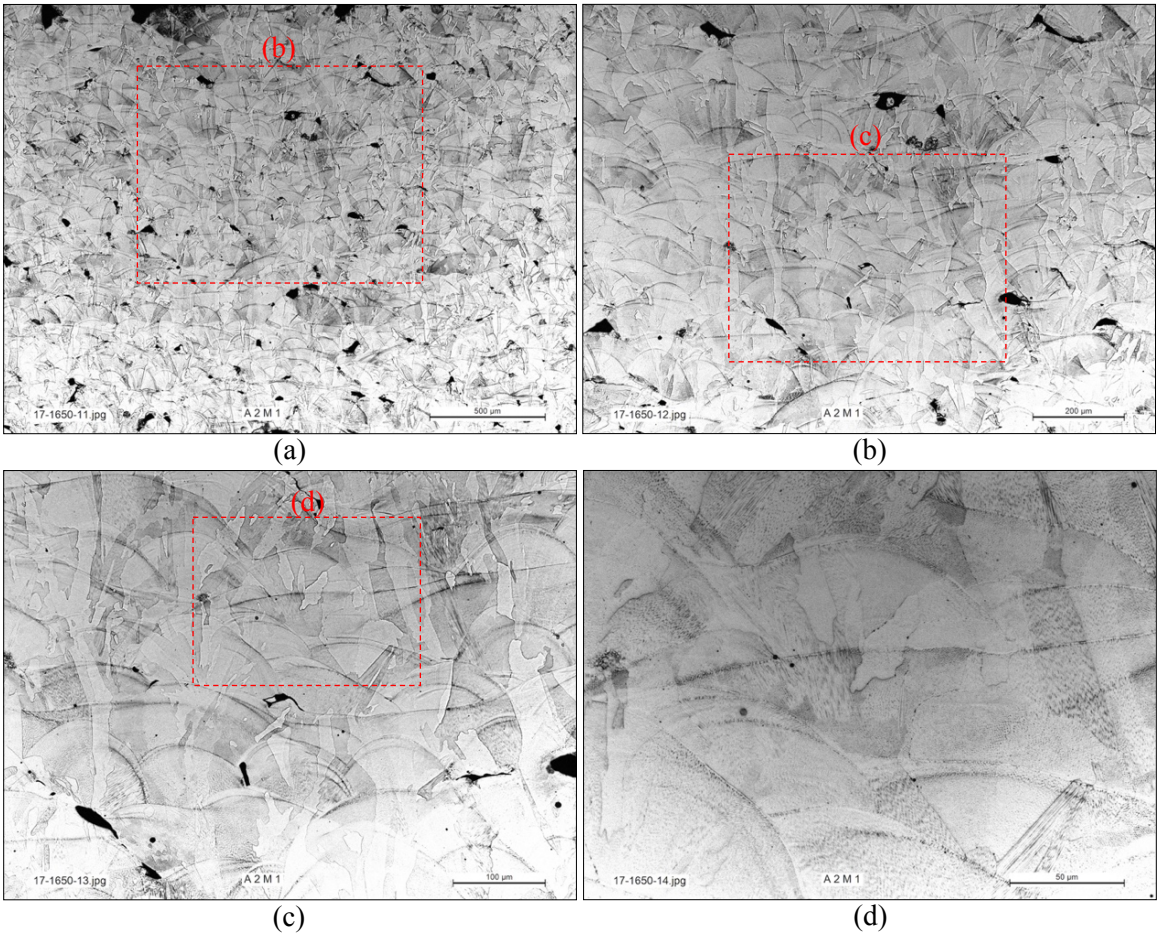

Figure 11. Optical images of specimen A2M1 from the as-fabricated swirl bubbler, the build direction is from the top to the bottom of the image.

A typical microstructure of specimens from the bubbler that underwent the HIPing consolidation treatment is shown in Figure 13 (b). The microstructure of the HIPed bubbler is quite different compared to the as-fabricated microstructure shown in Figure 13 (a). While some porosity was observed in the HIPed microstructure, the consolidated microstructure shows no structural artifacts from the SLM process, and looks very similar to a typical microstructure from rolled plate 316L produced using conventional steel-making processes.

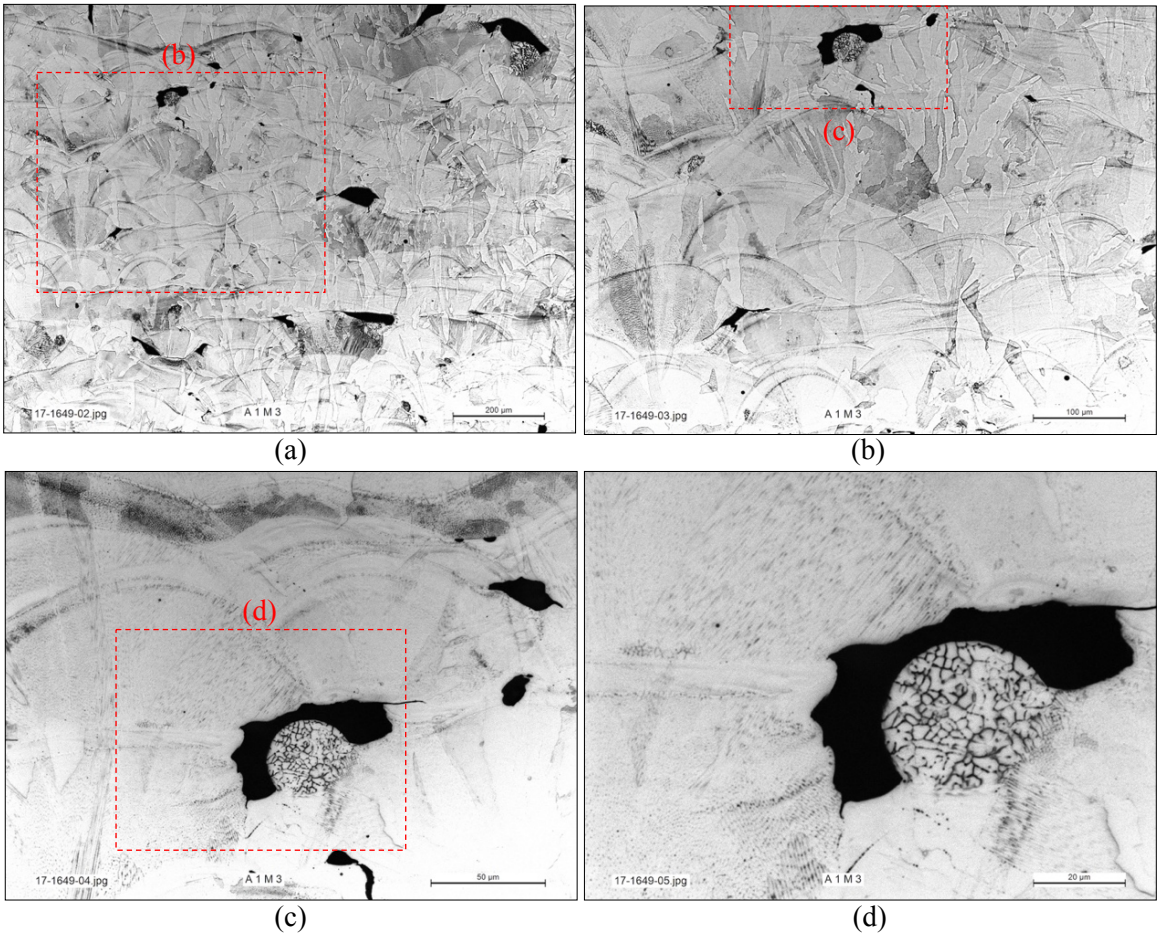

Figure 12. Optical images of the as-fabricated microstructure in specimen A1M3 illustrating a region with a cavity containing a partially fused powder particle.

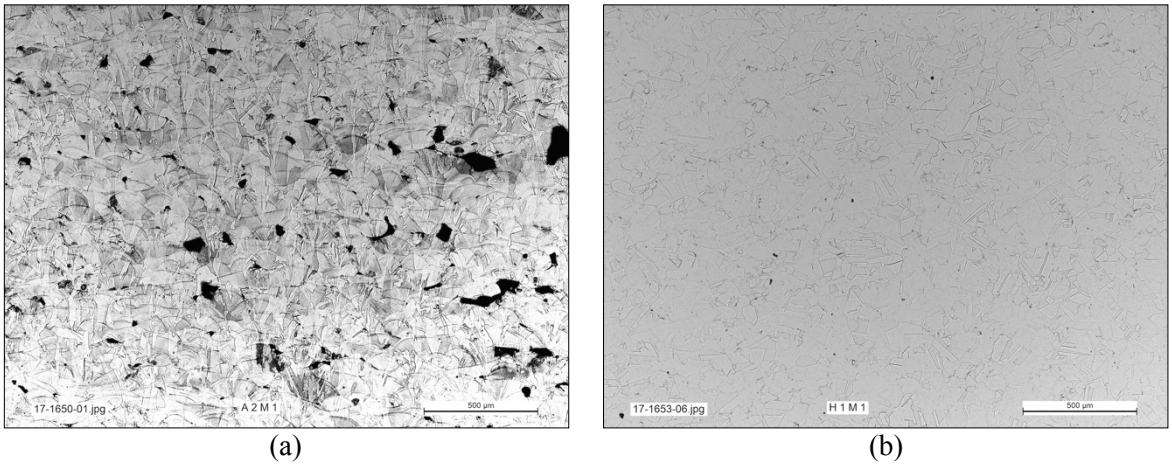

Figure 13. Optical images of the microstructure from specimens fabricated from (a) the as-fabricated and (b) HIPed bubbler assemblies. Note – these images are at the same magnification level.

The percent area of porosity was determined for each specimen using image analysis software to select the regions of porosity, as shown in Figure 14, and calculate the area fraction of porosity to the total area analyzed. The percent area of porosity for each specimens is shown in Table 3. Percent porosity for the specimens from the as-fabricated bubbler ranged from 2.2 to 6.2%, and the average porosity for the six specimens examined was approximately 4%.

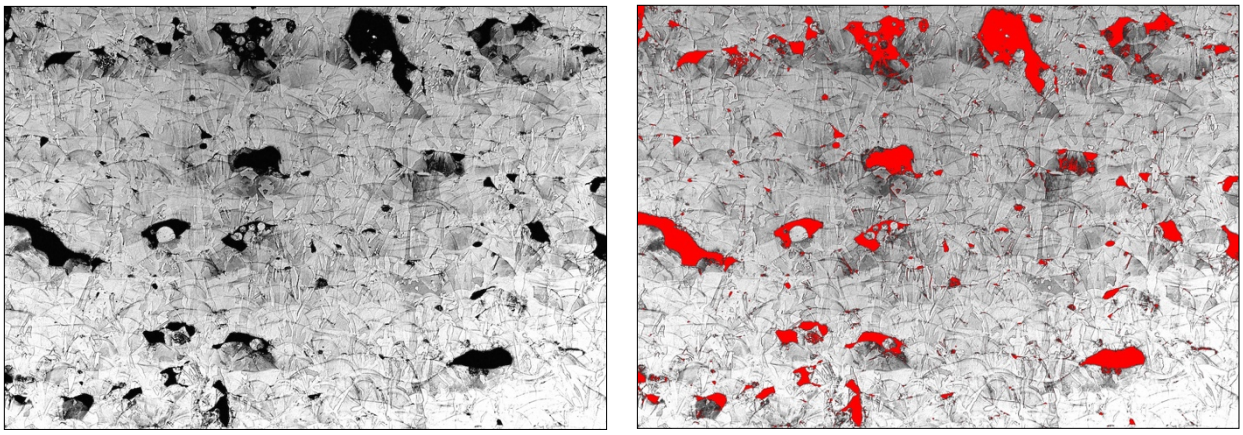

(a) (b)

Figure 14. (a) Optical image of a region in specimen A1M2 and (b) the same image with the microstructure porosity highlighted with red, which represents the area used for porosity calculations.

Condition	Specimen	Total Area Analyzed [µm²]	Area of Porosity [µm²]	Porosity [%]	Average Porosity [%]
As-Fabricated	A1M1	4344279	96579	2.22	4.04
	A1M2	4346692	267661	6.16	
	A1M3	4344279	177102	4.08	
	A2M1	4346692	124765	2.87	
	A2M2	4346692	202444	4.66	
	A2M3	4341867	184426	4.25	
After HIPing	H1M1	4346692	869	0.020	0.040
	H1M2	4341867	738	0.017	
	H1M3	4341867	1770	0.041	
	H2M1	4344279	1603	0.037	
	H2M2	4344279	3385	0.078	
	H2M3	4344279	1939	0.045	

Table 3. Porosity calculations for the as-fabricated and HIPed specimens.

Porosity of the specimens from the HIPed bubbler were approximately 0.04%, which is two orders of magnitude lower than porosity calculated for specimens from the as-fabricated bubbler assembly. These results illustrate why microstructure consolidation with HIPing is usually performed on components produced by SLM, that is, to reduce the porosity and decrease microstructural features that could serve as nucleation sites for crack formation and grow, which increases the material ductility and fatigue resistance.

3.2 TENSILE CHARACTERIZATION

The different microstructures of the two conditions observed during microscopy produced significantly different tensile properties, as shown in Table 4.

Condition	Specimen ID	Yield Strength [MPa]	Ultimate Strength [MPa]	Failure Stress [MPa]	Uniform Elongation [%]	Total Elongation [%]
As-fabricated	A1T9	340	354	297	0.51	1.40
	A1T10	387	396	377	0.39	0.76
	A1T11	442	483	434	1.54	2.95
	A1T12	410	424	411	0.55	0.90
	A1T13	345	346	266	0.22	1.35
	A2T9	322	330	212	0.39	2.16
	A2T10	423	459	346	1.19	3.13
	A2T11	270	272	134	0.13	1.81
	A2T13	389	417	104	0.88	5.22
	A1T8	344	345	326	0.26	0.62
	A1T7	409	468	435	2.70	3.76
	A1T5	365	369	345	0.34	0.74
	A2T5	379	414	295	0.88	2.47
	A2T6	362	371	361	0.34	0.54
	A2T8	331	351	335	0.95	1.26
	A1T1	414	418	399	0.26	0.62
	A1T2	254	258	233	0.11	0.50
	A1T4	447	486	121	2.18	9.56
	A2T1	201	202	189	0.29	0.62
	A2T2	225	228	213	0.11	0.37
	A2T4	365	399	201	1.42	5.52
After HIPing	H1T5	248	583	485	66.99	87.71
	H1T7	266	598	488	67.55	83.47
	H1T8	267	598	500	67.47	81.12
	H2T1	268	596	499	67.43	80.61
	H2T2	269	589	474	68.05	82.51
	H2T4	264	584	505	67.66	80.01
	H1T1	258	589	529	69.24	83.01
	H1T2	264	588	529	69.72	84.64
	H1T4	262	587	487	69.22	82.89
	H2T5	267	587	491	68.46	81.21
	H2T6	265	591	500	70.56	87.08
	H2T8	264	594	516	68.59	82.55
	H2T9	266	590	524	67.22	78.92
	H2T10	262	594	525	67.83	81.34
	H2T11	264	594	517	66.88	81.02
	H2T13	264	591	520	69.18	82.92
	H1T9	265	594	503	68.46	86.48
	H1T10	269	601	513	67.75	84.70
	H1T11	265	591	496	66.68	80.30
	H1T12	266	598	501	71.37	86.34
	H1T13	265	595	456	67.21	85.73

Table 4. Tensile testing results for the as-fabricated and HIPed bubbler assemblies.

Inconsistences in the microstructure from the porosity and lack-of-fusion defects produced inconsistences in the measured tensile properties. Yield and ultimate strength values measured for the as-fabricated and HIPed specimens are shown in Figure 15, where the disparity in scatter between the two conditions is clear. The as-fabricated specimens had significant scatter in the yield and ultimate strengths compare to the values measured for the HIPed specimens.

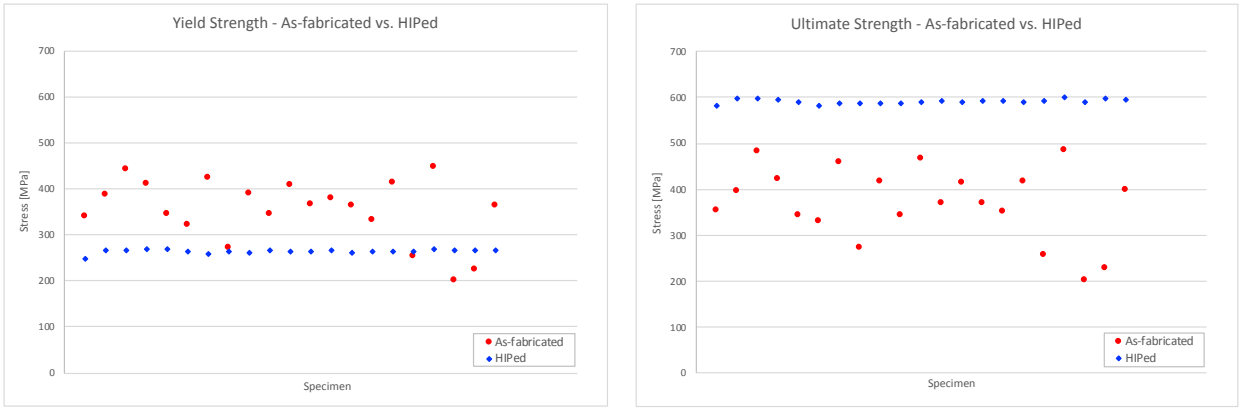

(a) (b)

Figure 15. (a) Yield and (b) ultimate strengths measured for tensile specimens fabricated from the as-fabricated and HIPed bubbler assemblies.

Yield strengths for the as-fabricated specimens ranged from ~200 to 450 MPa, whereas the yield strengths for the HIPed specimens ranged from ~250 to 270 MPa. Ultimate strength ranges were ~200 to 490 MPa and ~580 to 600 MPa for the as-fabricated and HIPed specimens, respectively. The low ultimate tensile strength values of the as-fabricated specimens show the material has low strain-hardening capability, and as a result the specimens experienced little plastic deformation before failure.

Discrepancies between the test results of the two material conditions was more pronounced for the ductility values. The uniform and total elongation values for the as-fabricated and HIPed specimens are shown in Figure 16. Uniform elongation range values were ~0.13 to 2.8% and 67 to 71% for the as-fabricated and HIPed specimens, respectively. Total elongation values were 0.37 to 9.56% and 79 to 88% for the as-fabricated and HIPed specimens, respectively. The low ductility levels of the as-fabricated are a result of the complex microstructure produced by the SLM process. Lack-of-fusion defects inhibit dislocation motion, deformation between adjacent grain boundaries, and severely decrease the ability of the material to plastically deform. Also the numerous crack initiation sites found in areas of the microstructure with lack-of-fusion defects promote fast fracture of the material rather than gradual plastic deformation with strain-induced hardening.

The tensile test results for the as-fabricated material illustrate why components produced from SLM are commonly consolidated using HIPing. Strength and elongation values for 316L are specified in ASTM-A240, which is the material standard utilized for the SNS target vessel material, and provide a reference for minimally acceptable mechanical properties for steel-mill fabricated 316L plate material.

The minimal yield and ultimate tensile strength values listed in ASTM-A240 for 316L are 170 and 485 MPa [16], respectively. The lowest yield and ultimate strength values measured for the HIPed specimens

were 250 and 580 MPa, respectively, well above the minimal requirements listed for rolled 316L plate material. The minimal total elongation value listed in ASTM A240 for 316L is 40% [16]. The lowest total elongation value measured for the HIPed specimens was approximately 79%, which is almost twice the minimal value specified for rolled 316L plate material. While the tensile values measured for the HIPed material surpasses the mechanical properties specified in ASTM A240, the fracture toughness and fatigue resistance of the SLM fabricated and HIPed bubbler assembly are not known. Further testing of fracture and fatigue resistance are recommended prior to utilizing bubbler assemblies produced via SLM and HIPing.

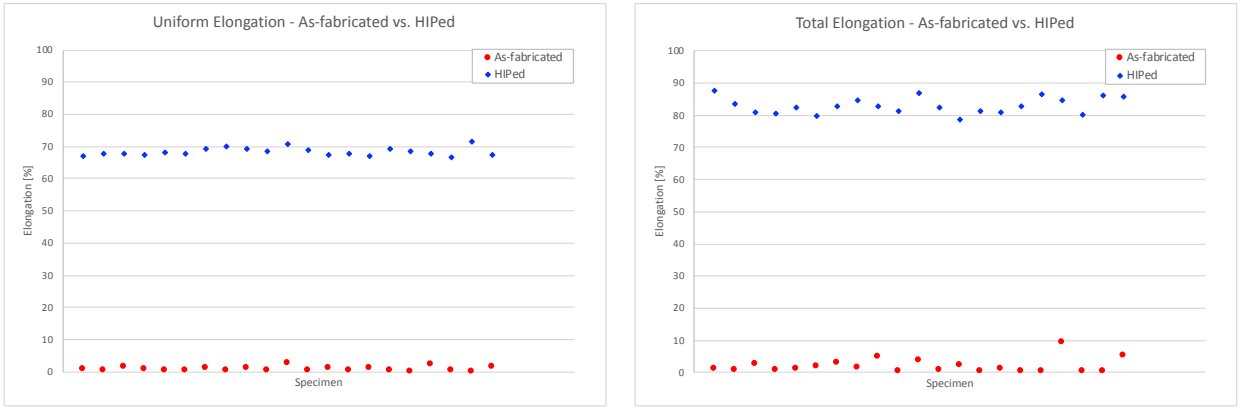

(a) (b)

Figure 16. (a) Uniform and (b) total elongation values measured for tensile specimens fabricated from the as-fabricated and HIPed bubbler assemblies.

4. SUMMARY AND CONCLUSIONS

Selective laser melting (SLM) was used to fabricate two swirl bubbler assemblies composed of 316L stainless steel. One bubbler assembly was consolidated using hot a isostatic pressing (HIPing) treatment and the other bubbler remained in the as-fabricated condition. Tensile and microstructure characterization specimens were fabricated from several areas of the bubbler assemblies to quantify the tensile properties and characterize the microstructure of the material with and without the HIPing treatment.

Metallography image show the two bubbler assemblies had significantly different microstructures. The as-fabricated microstructures has a fan shaped morphology, corresponding to the laser melt regions, and an appreciable number of lack-of-fusion defects. Spherical powder particles that did not completely melt during fabrication were observed in some lack-of-fusion cavities. Analysis of the microstructure images indicated that the percent porosity of the as-fabricated specimens averaged ~4%, whereas the porosity after HIPing averaged ~ 0.04%. Micrographs of the HIPed material show a microstructure similar in appearance to 316L in a plate form produced in a steel-mill.

Appreciable differences in tensile properties were observed for the two bubbler assemblies. The scatter in the results were much greater for the as-fabricated material compared to the HIPed material. Yield and ultimate strength values for the as-fabricated material ranged from ~200 to 450 MPa, respectively, whereas

the yield and ultimate strengths for the HIPed material ranged from ~250 to 270 MPa. Ultimate tensile strengths for the as-fabricated material ranged from ~200 to 490 MPa, respectively, while the ultimate strengths for the HIPed material ranged from ~580 to 600 MPa. Both the strength and elongation values measured for the HIPed plate were well above the values specified in ASTM A240 for annealed 316L in a plate form produced by traditional steel making processes in a mill.

The lack-of-fusion defects and poor tensile properties of the material in the as-fabricated condition are a cause for concern when considering this material condition for service in the SNS target vessel. However, the consolidated microstructure and excellent tensile properties observed for the SLM fabricated bubbler assembly after undergoing a HIPing treatment are promising. Tensile properties measured during testing are well above the material specification standard used for the SNS target vessel material and should be adequate for service in the SNS target. However, further investigations into the fracture toughness and fatigue resistance of the HIPed material are recommended prior to its use in an SNS target module during service.

5. REFERENCES

[1] J.R. Haines, B.W. Reimer, D.K. Felde, J.D. Hunn, S.J. Pawel, C.C. Tsai, Journal of Nuclear Materials 343 (2005) 58-69.

[2] K. Kikuchi, H. Kogawa, M. Futakawa, S. Ishikura, M. Kaminaga, R. Hino, Journal of Nuclear Materials 318 (2003) 84-91.

[3] B.W. Riemer, J.R. Haines, J.D. Hunn, D.C. Lousteau, T.J. McManamy, C.C. Tsai, J. Nucl. Mater. 318 (2003) 92-101.

[4] J.D. Hunn, B.W. Riemer, C.C. Tsai, Journal of Nuclear Materials 318 (2003) 102-108.

[5] S.J. Pawel, E.T. Manneschmidt, Journal of Nuclear Materials 318 (2003) 122-131.

[6] M.D. Kass, J.H. Whealton, N.E. Clapp Jr., J.R. DiStefano, J.H. DeVan, J.R. Haines, M.A. Akerman and T.A. Gabriel, Tribology Letters 5 (1998) 231-234.

[7] S.J. Pawel, Journal of Nuclear Materials 343 (2005) 101-115.

[8] B.W. Riemer et al., Journal of Nuclear Materials 377 (2008) 162-173.

[9] B.W. Riemer, M.W. Wendel, and D.K. Felde, Journal of Nuclear Materials 398 (2010) 207-209.

[10] Bernard W. Riemer, Mark W. Wendel, David K. Felde, Ashraf A. Abdou, and David A. McClintock, Journal of Nuclear Materials 431 (2012) 160-171.

[11] David Felde, Bernard Riemer, and Mark Wendel, Journal of Nuclear Materials 377 (2008) 155-161.

[12] B.W. Riemer et al., Journal of Nuclear Materials 450 (2014) 192-203.

[13] Takashi Naoe, Masato Ida, Masatoshi Futakawa, Nuclear Instruments & Methods in Physics Research A 586 (2008) 382-386.

[14] H. Kogawa. T. Naoe, H. Kinoshita, M. Ida, M. Futakawa, Development of bubbler injection technique in JSNS mercury target, in: Proceedings of ICANS XIX, 19th Meeting on Collaboration of Advanced Neutron Sources, Grindelwald, Switzerland TO047, March 8-12, 2010.

[15] Wim Blokland, Yun Liu, Mark Wendel, Drew Winder, *Measurements of the Effects of Gas Injection into SNS Target 18*, ORNL Technical Report 106010101-TR0043, December 2017.

[16] ASTM A-240/A240M – 10, *Standard Specification for Chromium and Chromium-Nickel Stainless Steel Plate, Sheet, and Strip for Pressure Vessels and for General Applications*, ASTM International 2010.

6. ACKNOWLEDGMENTS

The authors wish to thank Fredrick List III and Keith Carver at the Manufacturing Demonstration Facility (Oak Ridge, TN) for their guidance and support throughout the fabrication and analysis of the SNS target swirl bubblers.

7. APPENDIX A

Specimen Machining Maps for SNS Swirl Bubblers

David McClintock

Thao Strong

April 25, 2017

ORNL is managed by UT-Battelle
for the US Department of Energy

OAK RIDGE National Laboratory

Overview of Specimen Machining

- Specimens will be machined from <u>two</u> SNS bubbler assemblies
  - One assembly was provided as-manufactured and has metallic appearance
  - One assembly was HIPped and has a green appearance
- Two types of specimens will be fabricated from the assemblies
  - Tensile specimens
  - Microstructure characterization specimens
- All specimens will receive a unique identification number that will is determined by where the specimen was originally located in bubbler assembly
- Each bubbler assembly will be sectioned in half via wire-EDM prior to subsequent machining operations – specimens will be fabricated from only one half of each assembly

OAK RIDGE National Laboratory

Specimen Identification Scheme

- Each specimen will be assigned and labeled with a unique identification number
- Identifications will consist of four parts: **(1)** assembly ID, **(2)** quadrant number, **(3)** type of specimen, and **(4)** specimen number

Example – The second tensile specimen from Quadrant 1 of the as-received assembly will be labeled as follows:

A 1 T 2

Assembly ID:	Quadrant Region:	Type of Specimen:	Specimen Number:
A = As-received (metal color) **H** = HIPed (green color)	**1** = Quadrant 1 **2** = Quadrant 2	**T** = Tensile Specimen **M** = microstructure Specimen	**1**, **2**, **3**,…

OAK RIDGE National Laboratory

Specimen identification method and location

- Specimen identification must be applied with permanent method, such as laser marking or engraving
- Tensile specimens must be labeled on each specimen "head" as shown below – DO NOT apply label in or near specimen gauge section

Tensile Specimen

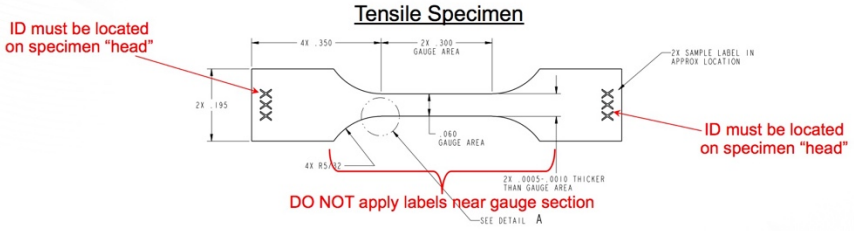

Microstructure Specimen

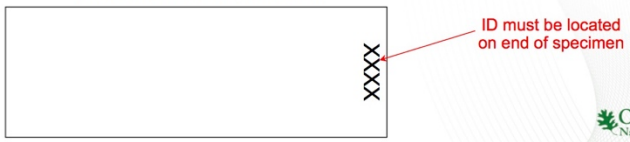

OAK RIDGE National Laboratory

Tensile Specimen Design

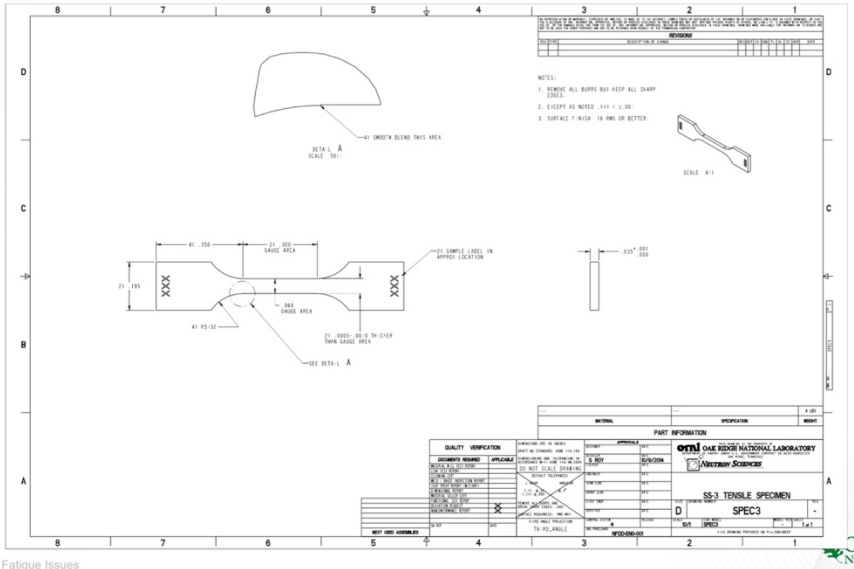

OAK RIDGE National Laboratory

Microstructure Specimen Design

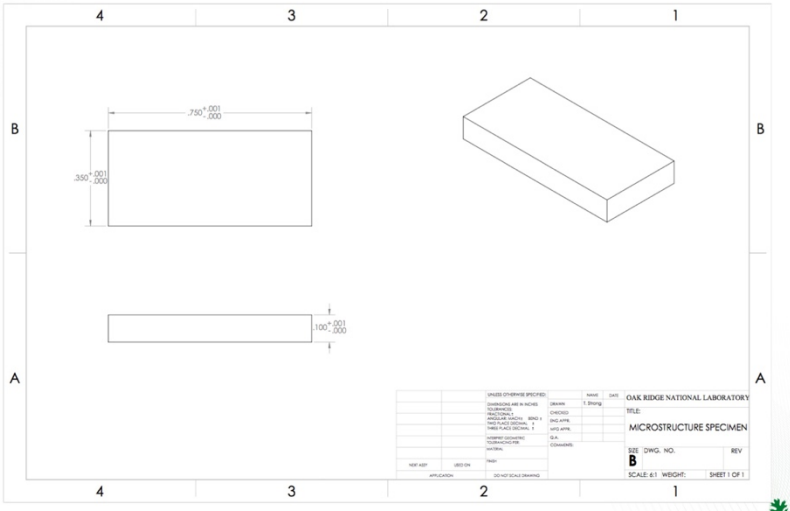

OAK RIDGE National Laboratory

Definition of Quadrants - View from top down (xy plane)

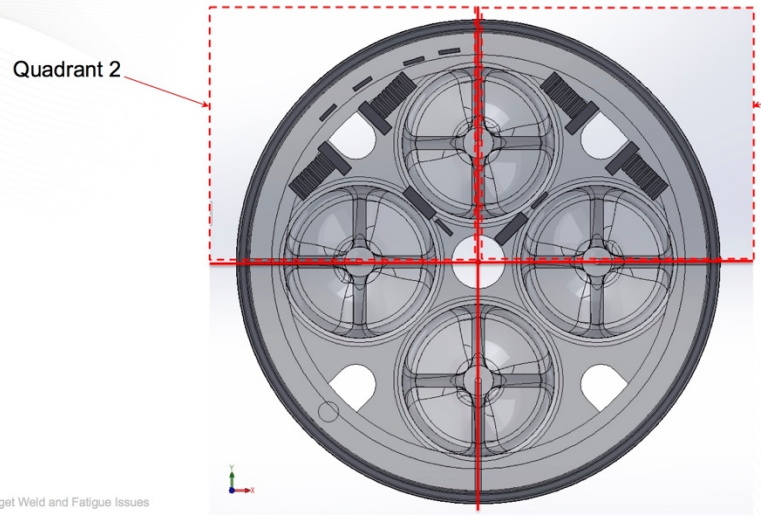

OAK RIDGE National Laboratory

Assemblies will be sectioned in half prior to specimen fabrication

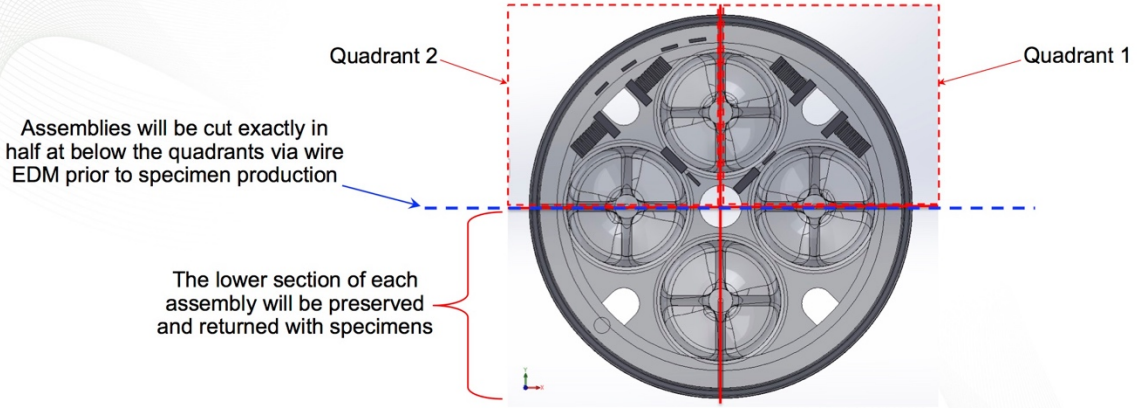

OAK RIDGE National Laboratory

Specimens will be machined from two different layers of the assemblies

- Specimens from the bubbler assemblies will be machined from two different elevations or "layers": (1) a "Top" layer and (2) a "Lower" layer

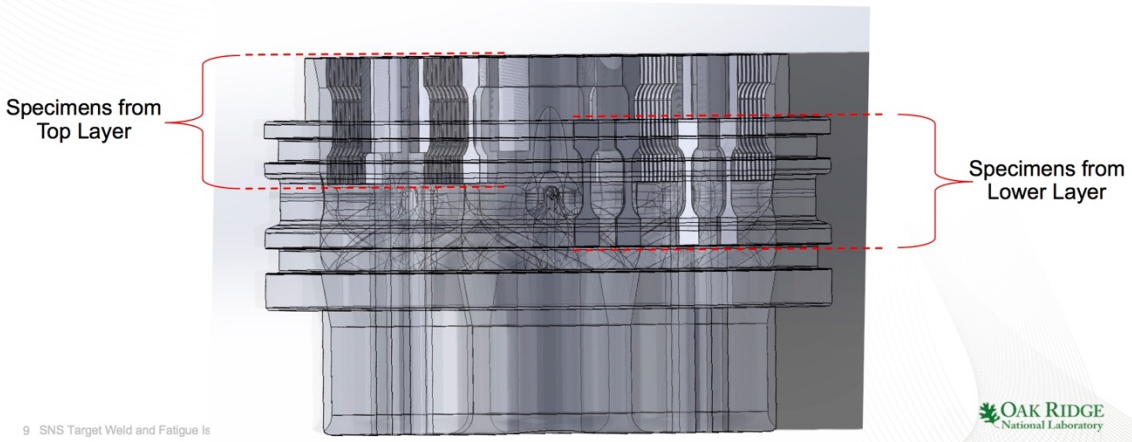

OAK RIDGE National Laboratory

Identification numbers and locations for specimens from top layer of as-fabricated assembly

*Tensile specimen positions are indicated by blue rectangles, ignore black rectangles between specimens

= *tensile specimen
= microstructure specimen

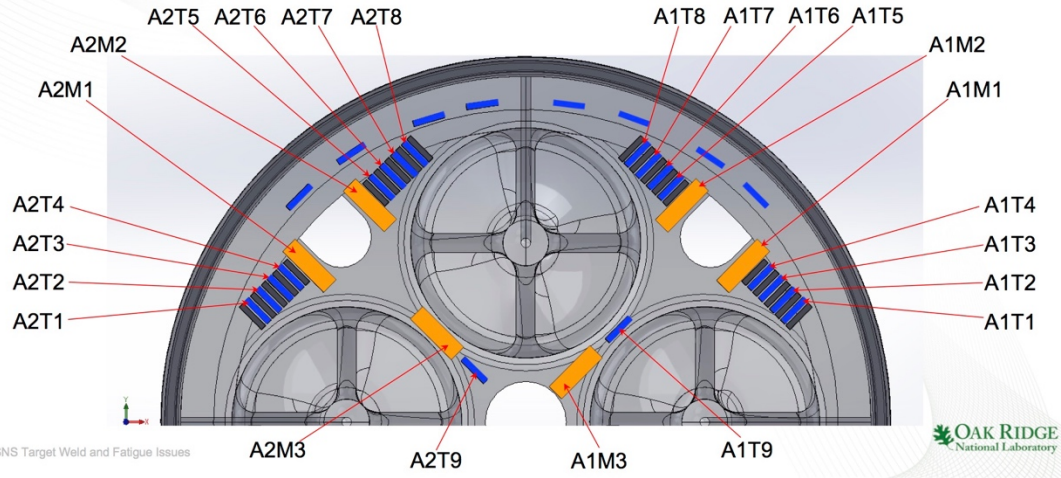

OAK RIDGE National Laboratory

Identification numbers and locations for specimens from lower layer of as-fabricated assembly

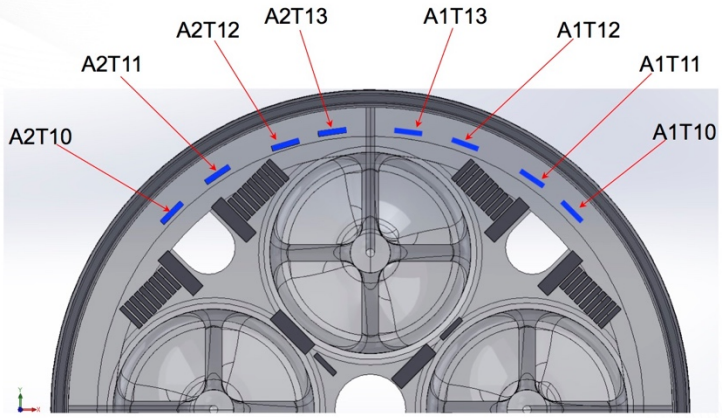

OAK RIDGE National Laboratory

Identification numbers and locations for specimens from top layer of HIPed assembly

*Tensile specimen positions are indicated by blue rectangles, ignore black rectangles between specimens

= *tensile specimen
= microstructure specimen

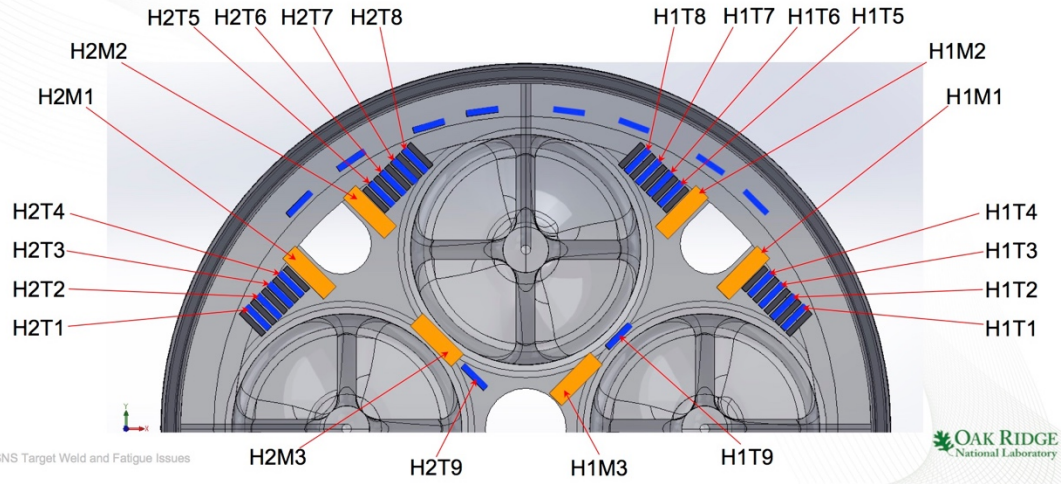

OAK RIDGE National Laboratory

Identification numbers and locations for specimens from lower layer of HIPed assembly

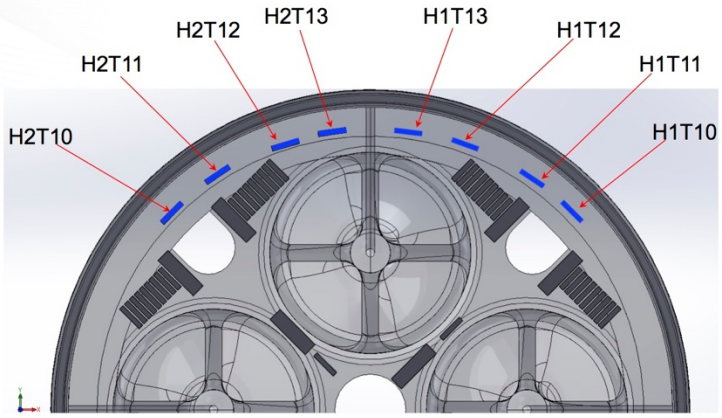

OAK RIDGE National Laboratory

Deliverables

- From the As-fabricated assembly: (1) 26 tensile and (2) 6 metallography specimens
- From the HIPed assembly: (1) 26 tensile and (2) 6 metallography specimens
- Two half-sections from the two assemblies

- Summary of Deliverables:
  - 52 tensile specimens
  - 12 microstructure specimens
  - Half section of as-fabricated assembly
  - Half section of HIPed assembly
  - All assembly scrap pieces from the machining process

OAK RIDGE National Laboratory

Miscellaneous Views of Assemblies

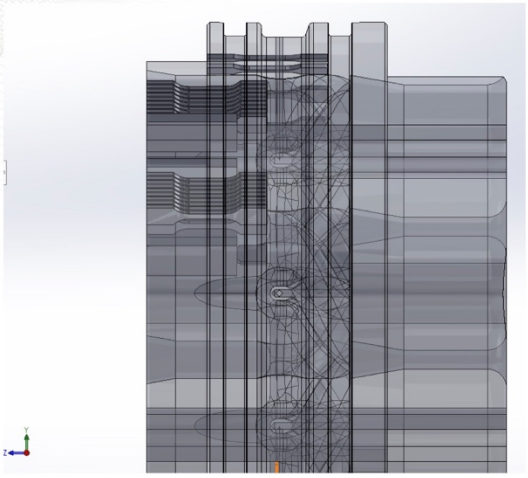

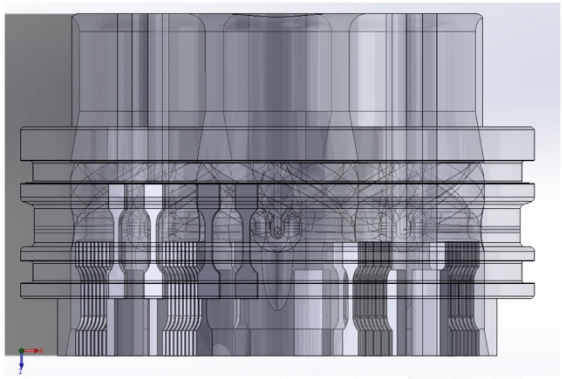

OAK RIDGE National Laboratory

Miscellaneous Views of Assemblies

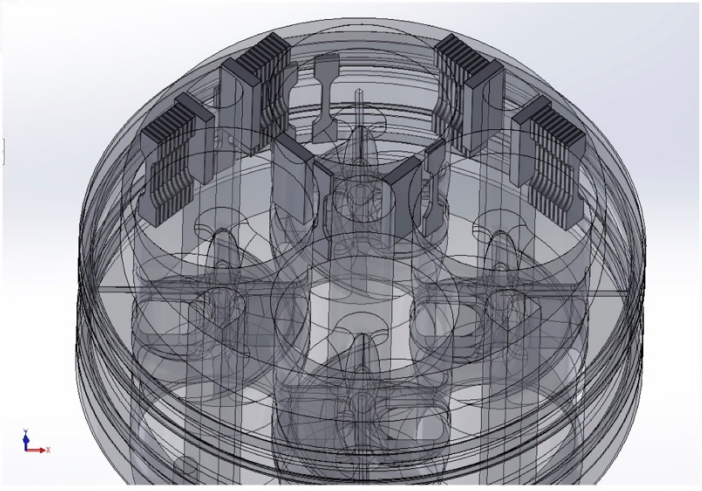

OAK RIDGE National Laboratory

Miscellaneous Views of Assemblies

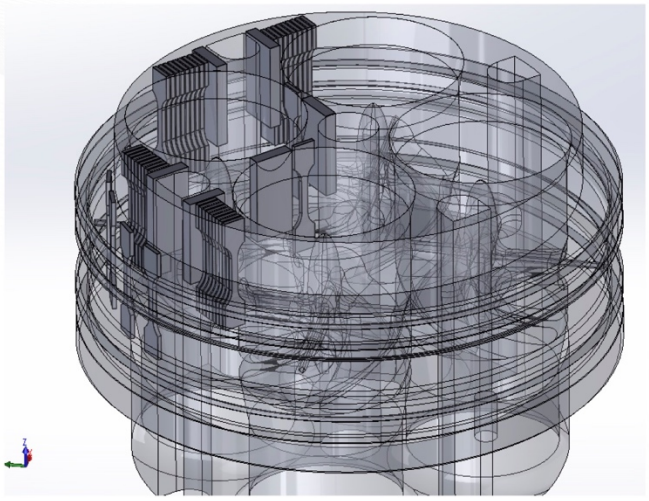

OAK RIDGE National Laboratory

Miscellaneous Views of Assemblies

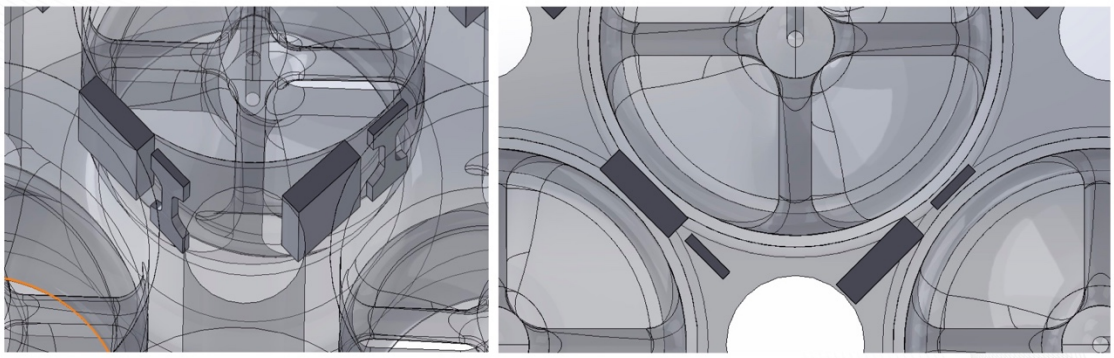

OAK RIDGE National Laboratory

Miscellaneous Views of Assemblies - Quadrant 2

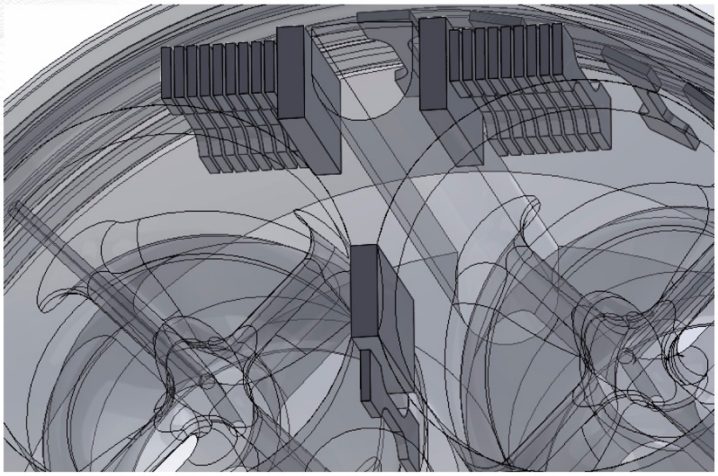

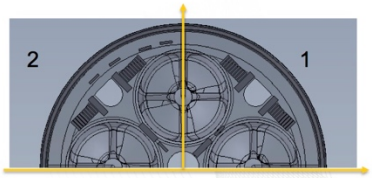

Miscellaneous Views of Assemblies - Quadrant 1